The Journal of Energy: Engineering & Management
Vol. 11, No. 4, Winter 2022, P. 48-59
Research Article

[DOR: 20.1001.1.23452951.1400.11.4.6.5]
[DOI: 10.22052.11.4.48]

Fault Location and Classification in non-Homogeneous Transmission Line Utilizing Breaker Transients

Zahra Moravej[1*], Pouriya Boostani[2], Mehrdad Ghahremani[3]

[1] Faculty of electrical and computer engineering, Semnan University, Semnan, Iran
zmoravej@semnan.ac.ir
[2] Faculty of electrical and computer engineering, Semnan University, Semnan, Iran
pouriya.boostani@ semnan.ac.ir
[3] Faculty of electrical and computer engineering, Semnan University, Semnan, Iran
mehrdad_ghahremani@semnan.ac.ir

Received: 2/6/2021 **Accepted:**11/28/2021

Abstract

In this paper, a single-ended fault location method is presented based on a circuit breaker operation using the frequencies of traveling waves. The proposed method receives the required data from voltage traveling waves with the aid of Fast Fourier Transform (FFT) and Wavelet Transform. Then, the Artificial Neural Network (ANN) identifies the fault type and determines its location. For the evaluation of the proposed method, numerous simulations were done by varying parameters including fault resistance, fault inception angle, fault location, the presence of noise in waves, different sampling frequencies, and different structures of the power system in PSCAD/EMTDC software. Then, by using the matrix data obtained from voltage signals, the training process of the proposed algorithm is implemented in MATLAB software. The given results show the acceptable accuracy of the proposed technique in the classification of fault type and in the determination of fault location comparing with the previous studies. Also, the maximum error of the proposed method is 1.29 percent. It stands for the robustness of the proposed scheme and is higher than those of the previous studies in the situations that may affect fault identification process.

Keywords: Fault location, Fault classification, Frequency of traveling waves, Fast Fourier Transform, Artificial Neural Network.

* Corresponding author
**This article is a selected article in SGC 2020 Conference, which has been accepted after completion and evaluation.

[DOR: 20.1001.1.23452951.1400.11.4.6.5]

[DOI: 10.22052.11.4.48]

1. Introduction

In a complicated power system, the electric power generation and consumption centers are not close. Thus, transmission lines play an important role in transmitting power from generation centers to consumers. With the deregulation of the power system and a competitive power market, delivering continuous power to the consumer has become essential. Therefore, the transmission system is expected to operate uninterruptedly. The transmission lines are the main artery of the power grids for delivering electric energy to consumers. Since these lines are outdoor and in pass areas with different weather conditions, they are subject to various faults. Faults might threaten the security and stability of the grid. Thus, the location of these faults should be determined to preserve lines' accessibility and to increase network reliability. Therefore, determining fault location in transmission lines is one of the essential topics to reduce repair and maintenance times. Since most faults in aerial lines are transient, an autorecloser switch can be used to energize the line after a short time.

On the contrary, the faults of the buried cables are steady, and it is not safe to use autorecloser. Thus, detecting the fault location in a hybrid transmission line is important to enable or disable the autorecloser [1-2]. Various studies have been conducted in this context, and various methods have been presented.

One of the fault location methods is based on impedance. This method is very simple and does not require advanced equipment. Thus, it would impose fewer costs, but it is significantly affected by fault and power system conditions like loading conditions, dissimilar lines, branches of the network, DGs, the saturation of the current transformer, the fault type, and resistance. Thus, its accuracy in capacitor-compensated three-terminal lines would be very low.

In [3], a fault location algorithm has been used in transmission lines with UPFC compensators that detect the accurate location of the faults and the internal and external faults based on the phasor theory. The proposed method employs remote terminal measurements simultaneously as the inputs of the algorithm.

The authors of [4] have employed a location algorithm on three-terminal transmission lines in which the series capacitors are used as a compensator. The proposed scheme comprises positive, negative, and zero series circuits and analyzes the equations with boundary equations for various normal shunt faults and simultaneous information of the terminal. Various fault information classification steps of the mentioned method do not depend on fault location information.

In [5], the fault location algorithm has been introduced for double-circuit transmission lines (DCTLs) in which series capacitors are used as compensators. In the proposed scheme, phasor theory and simultaneous terminal data are employed. Also, in this method, the SC model information is used to determine fault location.

According to the phasor theory and using circuits with negative series components in [6], a fault location algorithm has been presented in DCTLs that is compensated using SVC. In this study, the current and the voltage of a terminal are used, and the mutual connection between two conductors is considered completely. The proposed scheme does not require information about the fault classification steps and its calculations for accurate fault location, and this is done by using formulas. One of the shortcomings of this method and this type of analysis is avoiding resistance fault while the internal three-phase fault occurs.

Another method is based on hybrid methods. In [7-8], an intelligent fault location algorithm in DCTLs with a series capacitor compensator has been used, which is based on hybrid methods, including experimental wavelet transform and Hilbert transform (HT) as well as the weighted randomized vector functional line network (WEVFLN). In this study, an efficient feature has been used to support the vector structure. The selected feature can standardize amplitude deviation, energy, Renyi entropy, and the crest function of the HT arrays. The algorithm presented in this study can be trained online. Therefore, it requires complicated hardware for training and learning, which is a disadvantage.

In [9], a new method has been presented for remote protection using series compensator capacitors for transmission lines. This method is a new combination of hyperbolic s transform (HST) and support vector machines (SVM) for detecting, classifying, and locating faults, which are three main aspects of the remote relays. HST is used to extract applicable features of the sampled signals of current and voltage. The features extracted from the current and from the voltage of the sampled signals are used for remote protection methods and the support vector classification and regression.

In [10], a fault location algorithm has been presented in three-terminal transmission lines compensated with STATCOM. The proposed method is based on the combination of deep neural networks and WT without requiring offline information of the lines. The sampling frequency of the current and of the voltage signals is 45Hz and requires more than 50000 segments for training and learning neural networks, which is its disadvantage.

In [11], the fault location algorithm is based on the analysis of time-frequency signal processing, called the hyperbolic transform. This scheme is implemented in transmission lines equipped with UPFC. Three types of

the features of the fault signals are extracted in one of the compensated lines. These features are classified as Type 1, Type 2, and Type 3, which are based on the fundamental frequency components of the signals, time-frequency information, and hidden statistical features. In the intelligent fault detection method, accurate estimation is provided by improving the hidden statistical features that include a new type of time-frequency characteristics.

Another method is based on travelling waves (TW). This method required a fault locator with a high sampling rate capable of signal processing to detect and analyze the transient waves; thus, it would impose higher costs than the impedance-based method. The advantage of this method is that it is not affected by network conditions, the fault type and resistance, the fault angle, noise, etc.

In [12], a fault location algorithm has been presented in three-terminal transmission lines compensated with series capacitors that operate based on the TW theory and discrete wavelet transform. In this reference, the information of one terminal is used as the sample for fault location. In this method, location problems in line compensation with series capacitors are solved using equation analysis techniques in the time domain, which is the first step in the fault level detection of the impedance method, and other approaches are employed at the remote terminal to solve the fault location problem and to find the exact fault.

In [13], a fault location algorithm has been presented in transmission lines compensated with SSSC that operates based on TW and WT. This algorithm is based on using the modal transform for sampling high-frequency current and voltage signals. In WT, employing the calculations of the current and voltage, TWs and low-frequency interferences with system and SSSC are avoided.

In [14], TWs' polarity and arrival time at the line terminal are used to determine the fault location. In [15], TT and S transforms are used to extract the information of TWs in a hybrid network, and the obtained information is used to train an SVM to determine the fault location. In [16], the times obtained by using the Gabor transform and waves propagation speed are utilized to calculate the distance, which is compared with the line length to determine the fault location.

The authors of [17] have employed the TWs' frequency and ELM to determine the fault location. Also, in [18], The main factors that reduce the accuracy of the TW-based fault location algorithm are those that affect propagation speed, line length, or recorded time. Among these factors the uncertainty of line parameters, the consideration of the transmission line as lossless, the severe attenuation of the waves and the inability to detect them, the delay of the communication channel and the synchronization system, and insufficient sampling frequency can be mentioned. Regarding other problems reported in these algorithms, determining the terminal close-in faults and the faults of the power system in which there is a short line adjacent to the main line can be mentioned. Table 1 illustrates different methods of fault analysis executed by different researchers over the years.

This study presents a method based on the frequency of TWs resulting from the performance of the circuit-breaker. FFT is used to determine the frequency of the waves. Also, WT is used in addition to the FFT to identify the fault type. The proposed method has two objectives:

1. Identifying the fault type and determining its location without knowing the propagation speed and TWs' time.
2. More efficient performance in determining fault location under specific conditions.

The given results show the acceptable accuracy of the proposed method in different conditions.

The structure of this paper is as follows: Section 2 studies the TW theory, Modal transform, and FFT. Section 3 describes the proposed method. Section 4 presents the test and the training results of the neural network under different conditions. Section 5 compares the proposed method with several single-ended methods having been introduced in the literature.

Table 1: Results obtained from the comparison of the literature in the field of fault location in lines

Ref	Method	Line structure	Number of measurement terminals (Synchronous and asynchronous)	Sampling frequency (k Hz)	Average of error (%)
[3]	Im	1-C, 2-T	2-SY	4	0.03
[4]	Im	1-C, 3-T	3-US	2.4	0.1
[5]	Im	2-C, 2-T	2-US	NA	0.15
[6]	Im	2-C, 2-T	1	NA	0.14
[7]	Hy	2-C, 2-T	1	1.6	0.16
[8]	Hy	2-C, 2-T	1	1.6	0.16
[9]	Hy	1-C, 2-T	1	2.5	0.1
[10]	Hy	1-C, 3-T	3-SY	40	0.09
[11]	Hy	1-C, 2-T	1	6	0.15
[12]	Tw	1-C, 3-T	1	333.3	0.16
[13]	Tw	1-C, 2-T	2-SY	100	0.6
[14]	Tw	2-C, 2-T	2-US	200	0.13
[15]	Tw	1-C, 2-T	1	500	0.17
[16]	Tw	2-C, 3-T	3	100	0.14

NA: Not Available, **C:** Circuit, **T:** Terminal, **Im:** Impedance, **Hy:** Hybrid, **Tw:** traveling waves, **Sy:** synchronous, **US:** un-synchronous

2. Fundamentals

2.1. Theory of Traveling Waves

The differential equations of the voltage and current in a transmission line with losses relative to x [19] are as follows:

[DOR: 20.1001.1.23452951.1400.11.4.6.5]
[DOI: 10.22052.11.4.48]

$$\frac{dU}{dx} = -(R + j\omega L)I = ZI \quad (1)$$

$$\frac{dI}{dx} = -(G + j\omega C)U = YU \quad (2)$$

where Z and Y are known as Impedance, and admittance are per unit length of line respectively. $R(\Omega)$ is the resistance per unit length; $L(m)$ is the inductance per unit length;; G ( ) is the conductance of the dielectric per unit length; $C(F)$ is the capacitance per unit length; j is the imaginary unit, and ω is the angular frequency.

By differentiating Eq. (1) and Eq. (2), and substituting and sorting the equations, Eq. (3) and Eq. (4) are obtained. These equations describe the voltage and current phasor changes along the line. By solving Eq. (3) and Eq. (4), Eq. (5) and Eq. (6) are obtained for voltage and current concerning x.

$$\frac{d^2U}{dx^2} = ZYU \quad (3)$$

$$\frac{d^2I}{dx^2} = YZI \quad (4)$$

$$U(x) = A_1 e^{-\gamma x} + A_2 e^{\gamma x} \quad (5)$$

$$I(x) = \frac{1}{Z_c}(A_1 e^{-\gamma x} - A_2 e^{\gamma x}) \quad (6)$$

Constants A_1, A_2 are determined using boundary conditions. Z_c and γ are known as characteristic impedance and propagation constant respectively [20].

$$Z_c = \frac{Z}{\gamma} = \sqrt{\frac{Z}{Y}} = \sqrt{\frac{R + j\omega L}{G + j\omega C}} \quad (7)$$

$$\gamma = \sqrt{ZY} = \sqrt{(R + j\omega L)(G + j\omega C)} \quad (8)$$

Also, γ can be shown as $\gamma=\alpha+j\beta$, where in this mode α and β are known as attenuation constant and phase constant respectively [21].

$$\alpha = \sqrt{\frac{1}{2}[(RG - \omega^2 LC) + \sqrt{(RG - \omega^2 LC)^2 + \omega^2 (LG + RC)^2}]} \quad (9)$$

$$\beta = \sqrt{\frac{1}{2}[(-RG + \omega^2 LC) + \sqrt{(RG - \omega^2 LC)^2 + \omega^2 (LG + RC)^2}]} \quad (10)$$

The propagation velocity of waves is calculated by equation (7).

$$\lambda = \frac{2\pi}{k} \quad (11)$$

$$v = \lambda f = \frac{2\pi f}{k} = \frac{\omega}{k} \quad (12)$$

where V is Wave velocity, λ is the distance between two sequential crests or troughs (or other equivalent points), and k is Wavenumber (the spatial frequency of the wave in radians per unit distance).

2.2. Modal Transformation

In a three-phase line, there is inductive and capacitive coupling between the phases. If the transmission line is transposed efficiently, the mutual coupling can be eliminated by multiplying the modal matrix by the current/voltage matrix. One of the modal matrices is the Clark transform [22].

$$\begin{bmatrix} U_0 \\ U_\alpha \\ U_\beta \end{bmatrix} = \frac{1}{\sqrt{3}} \begin{bmatrix} 1 & 1 & 1 \\ \sqrt{2} & -1/\sqrt{2} & -1/\sqrt{2} \\ 0 & \sqrt{3/2} & -\sqrt{3/2} \end{bmatrix} \begin{bmatrix} U_a \\ U_b \\ U_c \end{bmatrix} \quad (13)$$

In equation (8), U_a ,U_b and U_c are phase voltages. U_0 is known as the voltage component of the ground mode. Also, U_α and U_β are known as the voltage components of aerial or line mode.

2.3. Fast Fourier Transform (FFT)

Discrete Fourier Transform (DFT) is a process of order $O(N^2)$. It is a process in which DFT is calculated as an $O(N\text{Log}_2 N)$ known as the Fast Fourier Transform [23]. In general, FFT is an extension of DFT, which differs in velocity and samples. FFT is faster in computations than DFT and requires its number of samples (N) to be a power of 2 (2^n).

3. Proposed Method

According to Eq. (5) and Eq. (6), the current and voltage TWs propagating in the transmission lines are attenuated with a constant propagation factor. Also, considering Eq. (7), Eq. (8), and Eq. (12), it can be concluded that the high-frequency waves are propagated and attenuated faster than the low-frequency waves. In this method, the above results are deployed to determine the fault location.

If the fault location is close to the terminal in which the TW is measured, the high frequencies of the TW have lower attenuation; thus, the measured TW is high in frequency. As the distance from the fault location increases, the high frequencies are attenuated gradually, and the TW would be low in frequency. Therefore, the wave turns into a low-frequency wave. In other words, the measure TW is the function of the fault location. Fig. 1 shows the attenuation of frequencies for a BC fault.

[DOR: 20.1001.1.23452951.1400.11.4.6.5]
[DOI: 10.22052.11.4.48]

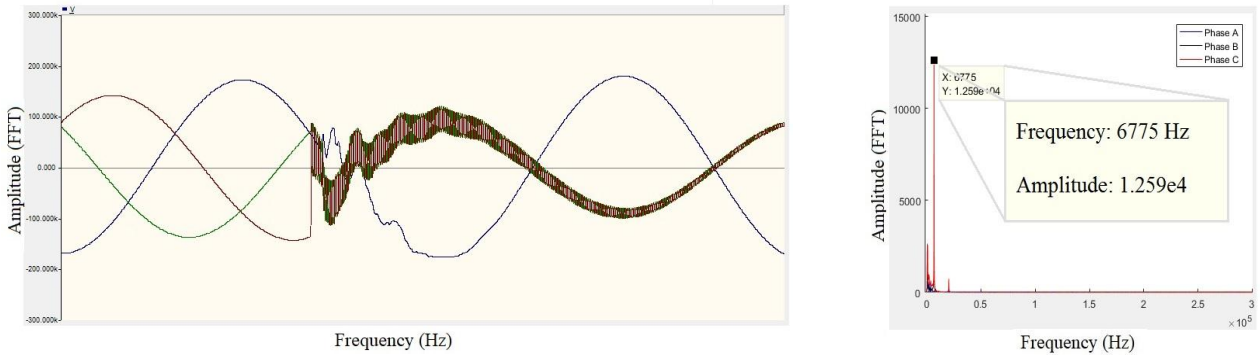

(a) Fault at 11 km and its related frequency

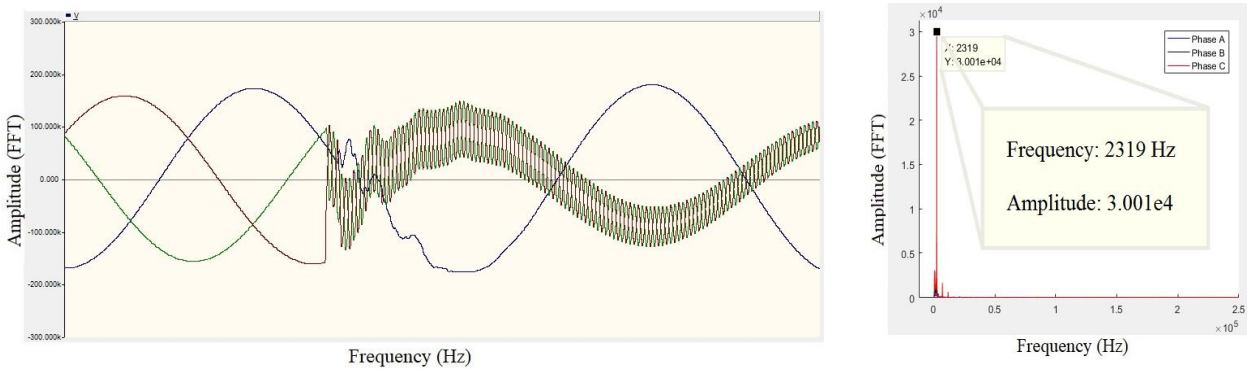

(b) Fault at 32 km and its related frequency

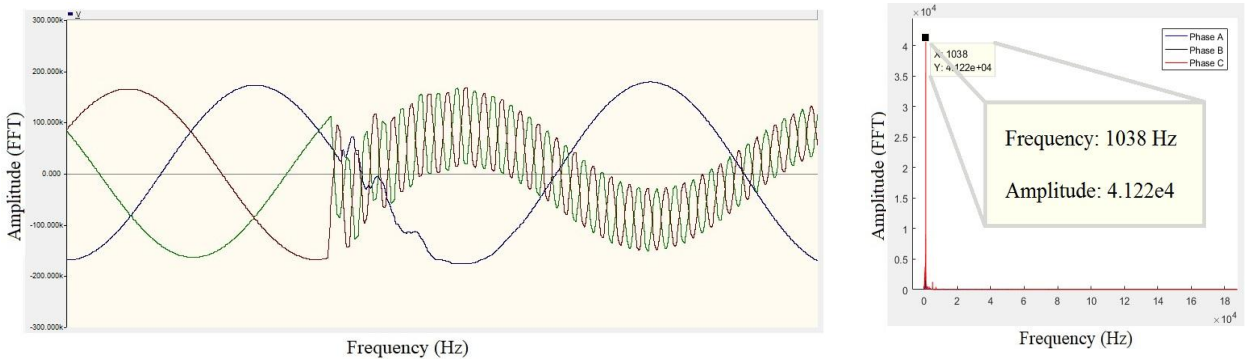

(c) Fault at 72 km and its related frequency

Fig. 1: Attenuation of frequencies as the fault point gets further away from terminal.

3.1. Recognition of Traveling Waves

Type-E single-ended method is used to detect and measure the travelling wave. The proposed method is based on the frequency of the transient voltages resulting from the operation of the circuit-breaker. When the protection relay detects a fault, it issues the command to disconnect the circuit-breaker. Upon the operation of the circuit-breaker and disconnection of the fault current, the TWs are propagated along the line. When the TW is reflected from the fault point and returns to the line terminal, it is measured and recorded. Then, its frequency is calculated to determine the fault type and its location, which are then given to the algorithm as input.

3.2. Classification of the Fault Type

As mentioned, the frequency of the TWs is required to detect the fault type. To this end, FFT is used. After sampling and filtering, the TWs are sampled with a frequency of 1MHz. Then, FFT is applied to determine the frequency of the waves and the amplitude of the frequencies.

If a phase is healthy, the frequency amplitude of its TW would be almost zero. On the contrary, if a phase is faulty, its frequency amplitude would be significant. Thus, the fault type can be detected by comparing the frequency amplitude of the phases. This method can detect 9 out of 11 possible faults. The above method can discriminate between the two-phase (LL) fault and the two-phase-to-ground (LLG) fault. To this end, WT is used. Therefore, in addition to FFT, WT is applied to TW.

First, the Clark transform is employed to remove the coupling between the phases; then, WT is applied to the

[DOR: 20.1001.1.23452951.1400.11.4.6.5]
[DOI: 10.22052.11.4.48]

ground mode obtained from the Clark transform.

If there exists the ground in the fault, the coefficient obtained from the WT applied to the ground mode would be significant; otherwise, the coefficient would be small [1]. Finally, the information obtained from FFT and WT is given to the neural network to detect the fault type.

3.3. Determination of the Fault Location

FFT alone is sufficient to determine the fault location. By applying this transform to the TW, the frequency and the frequency amplitude of the TW is obtained. Then, the obtained information is given to the neural network as input, and the fault location is determined. Fig. 2 shows a flow chart of the proposed method.

4. Simulation Result

A two-terminal 230kV power system with hybrid transmission power, including a 100Km aerial line and 10Km buried cable, is simulated in PSCAD/EMTDC. Fig. 3 shows the simulated power system. The configuration of the conductors in the aerial line and the buried cable is shown in Fig. 4. The related information about the understudy system is given in Table 11 in the appendix. A feed-forward multi-layer perceptron ANN is used here, which is trained by the information obtained from the faults assumed in the transmission system.

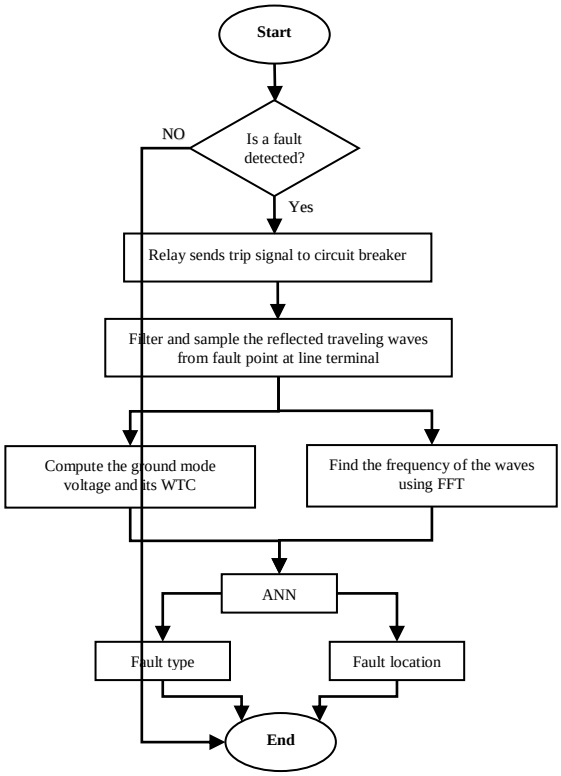

Fig. 2: Flowchart of the proposed method

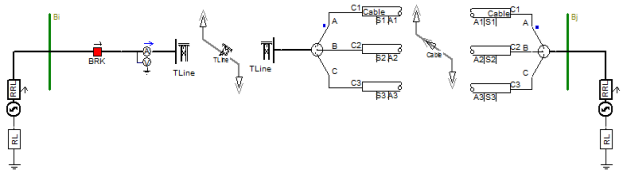

Fig. 3: Single line diagram of the simulated power system

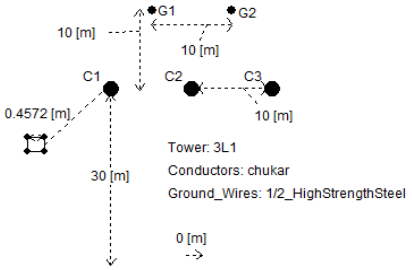

(a)

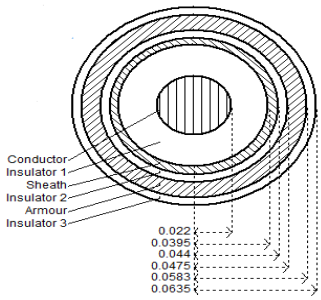

(b)

Fig. 4: Configuration of the conductors in overhead line and cables

4.1. Artificial Neural Network (ANN)

The ANN is assumed to be a three-layer network. The input layer contains 7 neurons as 7 inputs. Three inputs are the three-phase travelling waves, three other inputs include the amplitude of the frequencies, and the last input is the WT coefficient of the ground mode. The neural network has 3 hidden layers. The first hidden layer has 12 neurons, and the second layer has 6 neurons. The output layer also has two neurons, one for detection of the fault type and one for determining the fault location. Fig. 5 shows the diagram of the ANN; also, the related information is shown in Table 2.

Table 2: Related information to ANN layers

Layer	Neurons	Transfer function
Input	7	Sigmoid
First hidden layer	12	Sigmoid
Second hidden layer	6	Sigmoid
Output	2	Linear

[DOR: 20.1001.1.23452951.1400.11.4.6.5]
[DOI: 10.22052.11.4.48]

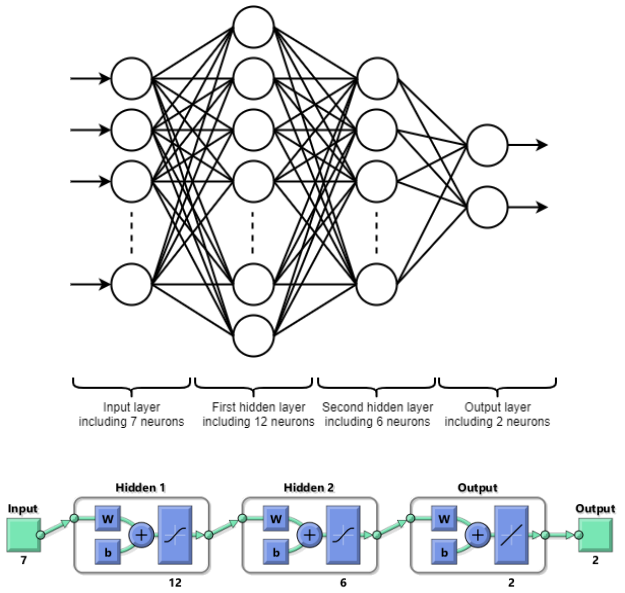

Fig. 5: Diagram of the ANN

4.1.1. Results of Training the ANN

Before training the neural network, a part of the data is used for training, and the other part is used for the test and validation. Then, the software starts training the network and testing the network while training and calculating its error. In the training process, 75% of the data (13221 data) is used for training, 15% (2644 data) is used for testing, and 10% of the data (1763 data) is used for validating the network. An optimization method should be used to obtain more realistic results. The optimization method employed in this process is the Levenberg-Marquardt method.

The results of training the neural network are shown in Fig. 6. According to this Fig., the training process is repeated 824 times, and it is terminated at the validation step after 6 errors. The initial MSE of the network is 510 and reaches the final value of 0.342 when the training process is finished. Therefore, the RMSE of the neural network is 0.584, and its accuracy is 99.416. Also, the final value of the error gradient is 2.38.

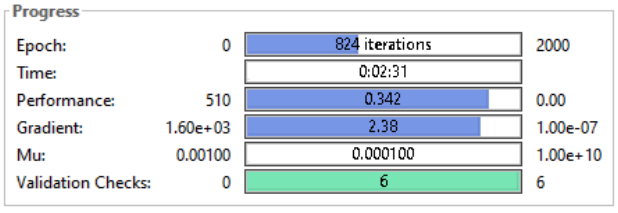

Fig. 6: The graph of MSE of trained ANN

Fig. 7 shows the reduction of MSE for training, for testing, and for validation data. According to this diagram, the best MSE is 0.306, which is obtained at the 818th iteration.

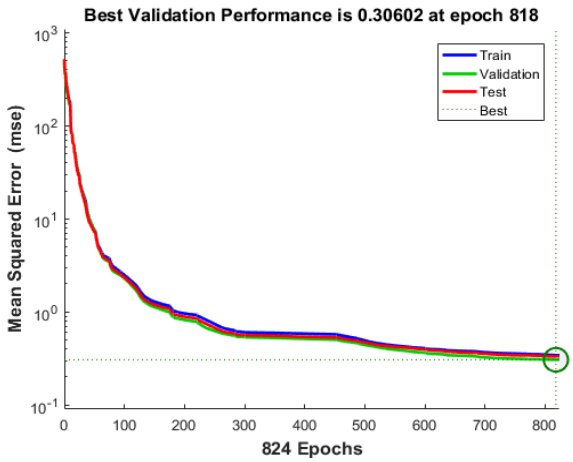

Fig. 7: The graph of MSE of trained ANN

Fig. 8 shows the regression of the neural network for training, validation, and testing data. As it can be seen, the total regression is 0.99983, which is close to 1.

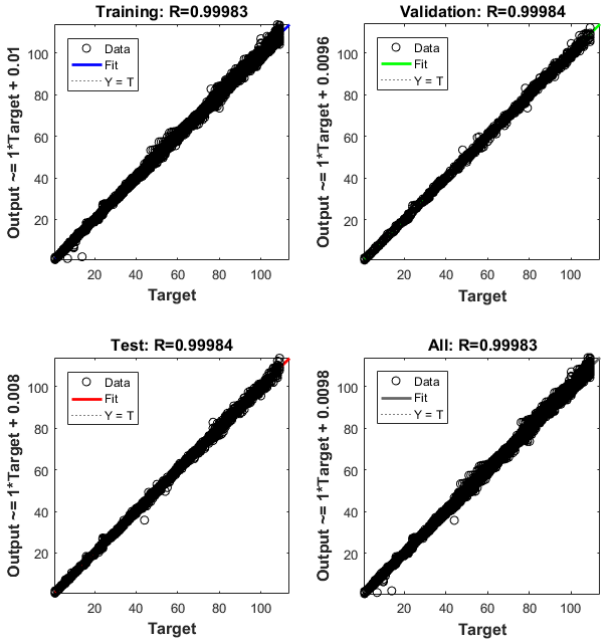

Fig. 8: Regression of the ANN

Fig. 9 shows the bar diagram of the training, of testing, and of validation data. In this figure, the line fault is assumed to be zero. It is seen that the error of each data set is about zero.

[DOR: 20.1001.1.23452951.1400.11.4.6.5]
[DOI: 10.22052.11.4.48]

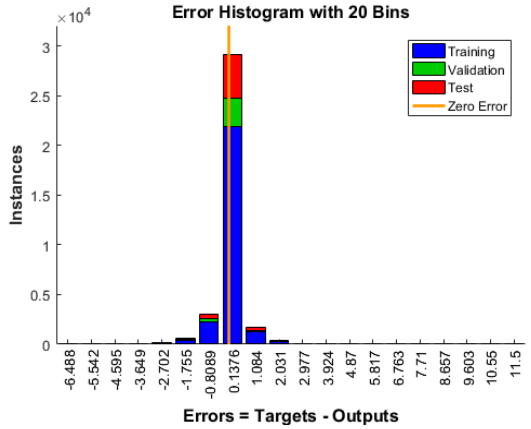

Fig. 9: the bar diagram of the training, test, and validation data.

Equation (9) is given for the calculation of the errors of calculation of the fault location in [28]. This formula is also used for the calculation of errors in this paper.

$$e_l = \frac{|m_m - m_t|}{L} \times 100 \qquad (14)$$

In the above-mentioned formula, m_m, m_t, and L are the fault locations determined by algorithm, actual fault location, and total length of line respectively. For testing the learned ANN, different data from the learning data are provided. The testing data are related to the following conditions:

4.2. Effect of Different Resistance, Inception Angle, the Type and the Location of Faults

The data related to 1000 faults with different conditions are obtained and delivered to ANN for testing. Some of the testing results are given in Table 3.

4.3. Effect of Close-in-faults

As mentioned, one of the specific conditions that challenge the fault location algorithms is determining the location of the faults close to the TW measurement terminal. According to Table 4, it can be concluded that the proposed method performs favorably under this condition.

4.4. Effect of Presence of Noise in Waves

The white noise function of MATLAB is used to generate noise in TW. The neural network is tested by the noise with two different SNR values which are 20 and 50 dB and are given in Table 5. The presence of noise does not affect the performance of the proposed method.

4.5. Effect of Different Sampling Frequencies

The 1MHz frequency is used for sampling the traveling waves. The 500 kHz and 750 kHz sampling frequencies are utilized to analyze the impact of sampling frequency on the accuracy of the proposed method. The size of the data window in the proposed method is 1/2 cycle. The results of this analysis are given in Table 6.

Table 3: Testing results of different fault resistance, inception angle, type and location

FT[1]	FR[2]	FI[3]	AFL[4]	DFL[5]	RFT[6]	RE[7]
AG	0.05	60	38	38.632	AG	0.574
AG	20	60	67	65.836	AG	1.058
AG	8	0	108	107.236	AG	0.694
BG	0.04	30	25	24.885	BG	0.104
BG	0.5	90	39	37.992	BG	0.916
BG	3	30	106.5	106.551	BG	0.047
CG	0.03	0	12	11.65	CG	0.317
CG	2	30	53	52.82	CG	0.162
CG	5	0	97	97.067	CG	0.061
AB	0.06	30	45	45.052	AB	0.047
AB	4	90	73	72.735	AB	0.24
AB	10	90	100	98.368	AC	1.483
BC	50	0	87	87.331	BC	0.301
BC	1	60	29	28.904	BC	0.086
BC	5	90	101	98.06	BC	2.675
AC	0.05	0	64	64.207	AC	0.188
AC	0.05	90	15	15.108	AC	0.099
AC	4	0	103	103.912	AC	0.83
ABG	0.2	30	71	70.807	ABG	0.174
ABG	5	30	103.5	103.419	ABG	0.073
ABG	11	60	34	33.986	ABG	0.012
BCG	0.06	90	91	89.533	BCG	1.333
BCG	2	30	41	40.931	BCG	0.062
BCG	2	90	105.5	106.92	BCG	1.291
ACG	0.04	60	18	17.847	ACG	0.138
ACG	1	0	51	50.885	ACG	0.104
ACG	1	60	81	80.907	ACG	0.084
ABC	0.1	90	90	90.038	ABC	0.035
ABC	7	90	22	22.044	ABC	0.04
ABC	10	0	103	104.546	ABC	1.405
ABCG	0.03	30	79	78.809	ABCG	0.173
ABCG	2	60	58	57.998	ABCG	0.001
ABCG	5	60	109	108.668	ABCG	0.301

FT[1]= Fault type, **FR[2]**= Fault resistance (Ω), **FI[3]**= Fault inception angle (degree), **AFL[4]**= Actual fault location (km), **DFL[5]**= Determined fault location (km), **RFT[6]**= Recognized fault type, **RE[7]**= Relative error (%)

Table 4: Testing results of close-in-faults

FT[1]	FR[2]	FI[3]	AFL[4]	DFL[5]	RFT[6]	RE[7]
AG	1	60	4	3.999	AG	0.0009
BG	3	30	2	1.937	BG	0.057
CG	2	0	6	5.808	CG	0.174
AB	10	90	1	0.931	AB	0.062
BC	1	0	8	7.907	BC	0.084
AC	0.05	0	9	8.975	AC	0.022
ABG	11	30	5	5.223	ABG	0.203
BCG	0.06	90	7	7.021	BCG	0.019
ACG	1	0	8	8.023	ACG	0.021
ABC	0.1	90	3	2.999	ABC	0.0009
ABCG	2	60	5	5.193	ABCG	0.175

[DOR: 20.1001.1.23452951.1400.11.4.6.5]
[DOI: 10.22052.11.4.48]

Table 5: Testing results of presence of noise in waves

FT[1]	FR[2]	FI[3]	AFL[4]	DFL[5]	RFT[6]	RE[7]
SNR = 20 dB						
AG	0.8	60	106	105.217	AG	0.711
BG	1	30	8	8.585	BG	0.532
CG	0.07	90	71	71.268	CG	0.243
AB	0.5	60	15	14.911	AB	0.08
BC	0.4	0	37	36.825	BC	0.158
AC	0.02	90	19	19.075	AC	0.068
ABG	0.6	60	58	57.7	ABG	0.272
BCG	0.1	30	12	12.054	BCG	0.049
ACG	0.09	0	87	87.453	ACG	0.412
ABC	50	60	30	30.846	ABC	0.77
ABCG	0.03	90	100	99.584	ABCG	0.377
SNR = 50 dB						
AG	1	30	4	3.897	AG	0.093
BG	3	60	33	32.719	BG	0.255
CG	20	30	52	52.763	CG	0.693
AB	0.7	30	107	104.62	AB	2.163
BC	0.1	0	10	9.944	BC	0.05
AC	7	60	70	69.901	AC	0.09
ABG	0.05	30	7	6.755	ABG	0.222
BCG	8.5	0	83	81.736	BCG	1.149
ACG	0.2	60	100	98.965	ACG	0.94
ABC	5	90	60	59.805	ABC	0.177
ABCG	2	60	108	107.494	ABCG	0.459

Table 6: Testing results of different sampling frequencies

FT[1]	FR[2]	FI[3]	AFL[4]	DFL[5]	RFT[6]	RE[7]
500 kHz						
AG	1	90	100	97.747	AG	2.048
BG	3	0	67	66.781	BG	0.198
CG	0.05	90	103	102.934	CG	0.059
AB	45	60	42	42.54	AB	0.472
BC	5	0	107	109.921	BC	2.656
AC	2.5	30	86	85.551	AC	0.408
ABG	0.5	30	18	18.241	ABG	0.218
BCG	30	90	20	19.891	BCG	0.01
ACG	3.5	0	6	5.777	ACG	0.202
ABC	0.06	30	105	107.156	ABC	1.96
ABCG	0.9	0	1	1.122	ABCG	0.111
750 kHz						
AG	20	0	23	22.502	AG	0.452
BG	0.1	90	4	3.742	BG	0.234
CG	4	30	10	10.439	CG	0.4
AB	6	60	101	100.144	AB	0.777
BC	0.2	30	35	34.861	BC	0.125
AC	0.03	60	5	4.87	AC	0.118
ABG	7	60	100	98.216	ABG	1.621
BCG	0.3	0	75	74.774	BCG	0.205
ACG	0.08	30	56	55.69	ACG	0.281
ABC	1	60	60	60.592	ABC	0.538
ABCG	5.5	90	106	106.247	ABCG	0.225

4.6. Effect of Adjacent Short Line

If the algorithm requires the wave arrival time, the sequential reflection of the TW from the short line terminal challenges the detection of the wave reflected from the fault point. According to Table 7, the short line simulated adjacent to the main line does not affect the neural network's performance.

Table 7: Testing results of adjacent short line

FT[1]	FR[2]	FI[3]	AFL[4]	DFL[5]	RFT[6]	RE[7]
AG	5	0	78	77.348	AG	0.592
BG	0.08	60	10	10.504	BG	0.458
CG	0.5	30	104	107.29	CG	2.993
AB	2	90	2	1.979	AB	0.019
BC	20	0	50	50.015	BC	0.013
AC	30	30	29	29.327	AC	0.297
ABG	10	90	55	54.324	ABG	0.614
BCG	50	60	98	98.509	BCG	0.462
ACG	0.8	0	17	17.008	ACG	0.007
ABC	4	30	100	99.4	ABC	0.546
ABCG	11	90	108	107.52	ABCG	0.429

4.7. Effect of Absence of Underground Cable

The ANN is trained using the fault information obtained from the power system shown in Fig. 2.

A 10Km aerial line is replaced by the buried cable to examine the changing of the structure of the power system. The results of the neural network under this condition are shown in Table 8. It is seen that changing the structure of the power system does not affect the performance of the proposed method.

Table 8: Testing results of absence of underground cable

FT[1]	FR[2]	FI[3]	AFL[4]	DFL[5]	RFT[6]	RE[7]
AG	0.02	30	2	2.411	AG	0.374
BG	0.6	0	32	31.428	BG	0.519
CG	50	30	100	100.306	CG	0.278
AB	5	0	102	100.21	AB	1.626
BC	0.07	30	12	11.945	BC	0.05
AC	5	90	75	74.754	AC	0.223
ABG	30	30	101	100.63	ABG	0.336
BCG	10	90	108	107.75	BCG	0.225
ACG	0.3	30	51	50.39	ACG	0.554
ABC	8	0	90	89.919	ABC	0.073
ABCG	10	30	104	104.11	ABCG	0.1

4.8. Effect of Double-circuit Line

To generalize the application of the proposed method and further investigation of changes in the power system structure, a double-circuit transmission line is considered. To this end, first, an aerial line of 10Km length is replaced by the buried cable. Then, the whole transmission line is simulated as a double-circuit line. According to Table 9, using a DCTL does not affect the performance of the ANN.

[DOR: 20.1001.1.23452951.1400.11.4.6.5]
[DOI: 10.22052.11.4.48]

[DOR: 20.1001.1.23452951.1400.11.4.6.5]

[DOI: 10.22052.11.4.48]

Table 9: Testing results of double-circuit line

FT[1]	FR[2]	FI[3]	AFL[4]	DFL[5]	RFT[6]	RE[7]
AG	1	30	12	11.736	AG	0.239
BG	0.07	90	40	39.46	BG	0.49
CG	50	60	22	21.025	CG	0.886
AB	5	60	8	7.87	AB	0.118
BC	0.09	90	32	31.974	BC	0.022
AC	30	90	100	97.882	AC	1.925
ABG	0.1	30	55	54.732	ABG	0.243
BCG	0.5	90	64	63.69	BCG	0.281
ACG	0.05	0	105	103.93	ACG	0.973
ABC	0.08	30	106	104.53	ABC	1.336
ABCG	7.5	60	86	85.096	ABCG	0.821

5. Comparisons

The proposed method is based on the frequency of the travelling waves, and FFT is used for this purpose. Therefore, unlike the methods presented in most papers, this method is independent of the arrival times of the waves and their propagation velocity. The methods that require wave propagation velocity and time, WT, TT, Park transform, TEO, and etc. are used to determine the waves' time. WT transform depends on parameters, including the mother function, number of decomposition levels, scale factor, and data window, which might affect its accuracy. Also, if the synchronization system is required, GPS system failure or delay might affect the times and result in an error. When a short line is adjacent to the main line, the reflection of the waves from its terminal challenges the detection of the wave reflected from the fault point.

Table 10: The comparison between proposed method and other methods

method	[1]	[14]	[15]	[16]	[17]	[18]	**Proposed method**
SF[1]	0.5	1	0.2	1.2	1	0.2	**0.5-1**
ME[2]	2	0.9	1.8	NR	1.3	1.2	**1.29**
S[3]	N	N	Y	Y	N	N	**N**
EFR[4]	R	R	R	R	R	R	**R**
EIA[5]	R	R	R	R	R	R	**R**
EFT[6]	R	R	R	R	R	R	**R**
HLC[7]	NR	NR	R	NR	NR	NR	**R**
EDCL[8]	NR	NR	NR	R	NR	NR	**R**
ESR[9]	NR	NR	NR	NR	NR	R	**R**
NI[10]	R	R	NR	R	NR	NR	**R**

SF[1]= Sampling frequency (MHz), **ME[2]=** Maximum error %, **S[3]=** Synchronization, **EFR[4]=** Effect of fault resistance, **EIA[5]=** Effect of inception angle, **EFT[6]=** Effect of fault type, **HLC[7]=** Hybrid line consideration, **EDCL[8]=** Effect of double circuit line, **ESR[9]=** Effect of sampling rate, **NI[10]=** Noise interference

N=No, **Y**=Yes, **NR**=Not reported, **R**= Reported

While the proposed method is independent of the arrival time of TWs, the short line does not affect its performance. In Table 10, some specific conditions considered in this paper are compared with some other studies.

6. Conclusions

In this paper, a method is presented to determine the fault location in a two-terminal network based on the frequency of TWs resulting from the operation of the circuit-breaker. The objectives of this study are detecting and determining the fault location under a specific condition, independent of wave propagation time and velocity. In this method, the frequency and frequency amplitude of TWs in all three phases and WTC of the ground mode are deployed to detect the fault type. The frequency and frequency amplitude of TWs of all three phases are required to determine the fault location. The information obtained from faults under various conditions is used to train a neural network. Then, the neural network is tested using various factors such as the fault type, fault resistance, the fault angle, and different fault locations, close-in faults, noise, short adjacent line, and power system structure to examine the efficiency of the proposed method .

The obtained results indicate the high accuracy of the proposed method in detecting fault type and determining its location. The only situation that can affect the accuracy of the proposed method is the presence of those faults that are adjacent to the connection point of the aerial line and the buried cable.

Appendix

Table 11: Related information to power sources

Source parameters				
Source	MVA	Voltage (kV)	Frequency (Hz)	δ (degree)
A	100	230	50	0
B	100	230	50	-20
Lines parameters				
OH line length			Cable length	
100km			11km	

Table 12: Values of resistance and inception angle of faults for ANN learning

Fault types	Fault resistances	Fault inception angles
AG, BG, CG, AB, BC, AC, ABG, BCG, ACG, ABC, ABCG	0.01, 0.1, 1, 5, 10, 50	0, 30, 60, 90

References

[1] George, N. and Naidu, O. D., "Traveling wave based autoreclosure scheme for multi-terminal lines", IEEE PES Innovative Smart Grid Technologies Conference Europe (ISGT-Europe), pp. 1-6, 2017.

[2] Mukherjee, A., Kundu, P. K. and Das, A., "Transmission line faults in power system and the different algorithms for identification, classification and localization: a brief review of methods", Journal of The Institution of Engineers (India): Series B, pp. 1-23, 2021.

[3] Chatterjee, A. and Debnath, S., "Sequence component-based approach for fault discrimination and fault location estimation in UPFC compensated transmission line", Electr. Power Syst. Res., Vol.180, 2020.

[4] Saffarian, A. and Abasi, M., "Fault location in series capacitor compensated three terminal transmission lines based on the analysis of voltage and current phasor equations and asynchronous data transfer", Electr. Power Syst. Res., Vol. 187, pp. 414-428, 2020.

[5] Cai, D. and Zhang, J., "New fault-location algorithm for series-compensated double-circuit transmission line", IEEE Access, Vol. 8, pp. 210685-94, 2020.

[6] Ghorbani, A. and Mehrjerdi, H., "Accurate fault location algorithm for shunt-compensated double circuit transmission lines using single end data", Int. J. Electr. Power Energy Syst., Vol. 116, 2020.

[7] Sahani, M. and Dash, P., "Fault location estimation for series-compensated double-circuit transmission line using parameter optimized variational mode decomposition and weighted P-norm random vector functional link network", Appl. Soft Comput., Vol. 85, pp. 1-18, 2019.

[8] Sahani, M. and Dash, P., "Fault location estimation for series-compensated double-circuit transmission line using EWT and weighted RVFLN", Eng. Appl. Artif. Intell, Vol. 88, Article No. 103336, 2020.

[9] Moravej, Z., Khederzadeh, M. and Pazoki, M., "New combined method for fault detection, classification, and location in series-compensated transmission line", Electr. Power Compon. Syst., Vol. 40, pp. 1050-71, 2012.

[10] Mirzaei, M., Vahidi, B. and Hosseinian, S., "Accurate fault location and faulted section determination based on deep learning for a parallel-compensated three-terminal transmission line", IET Gener. Transm. Distrib, Vol. 13, pp. 2770-78, 2019.

[11] Moravej, Z., Pazoki, M. and Khederzadeh, M., "New smart fault locator in compensated line with UPFC", Int. J. Electr. Power Energy Syst., Vol. 92, pp. 125-135, 2017.

[12] Evrenosoglu, A. and Abur, A., "Travelling wave based fault location for teed circuits", IEEE Trans. Power Delivery, Vol. 20, pp. 1115-21, 2005.

[13] Archundia, A. and Guardado, J. L., Morenogiytia, E. L., Gutierrez-Gnecchi, J. A. and Martinez-Cardenas, F., "Fault detection and localization in transmission lines with a static synchronous series compensator", Adv. Electr. Comput. Eng., Vol. 15, pp.17-22, 2015.

[14] Peng, N., Zhou, L., Liang, R. and Xu, H., "Fault location of transmission lines connecting with short branches based on polarity and arrival time of asynchronously recorded traveling waves", Electr. Power Syst. Res, Vol. 169, pp. 184-194, 2019.

[15] Gashteroodkhani, O. A., Majidi, M., Etezadi-Amoli, A. F. and Vahidi, B., "A hybrid SVM-TT transform-based method for fault location in hybrid transmission lines with underground cables Electr", Power Syst. Res, Vol. 170, pp. 205-214, 2019.

[16] Moravej Z., Movahhedneya, M. and Pazoki, M., "Gabor transform-based fault location method for multi-terminal transmission lines", Measurement, Vol. 125, pp. 667-679, 2018.

[17] Akmaz, D., Mamis, M. S., Arkan, M. and Tagluk, M. E., "Transmission line fault location using traveling wave frequencies and extreme learning machine", Electr. Power Syst. Res, Vol. 155, pp. 1-7, 2018.

[18] Deng, F., Zeng, X., Tang, X., Li, Z., Zu, Y. and Mei, L., "Transmission lines using three-dimensional absolute grey incidence degree", Int. J. Electr. Power Energy Syst., Vol. 114, 2020.

[19] Shenkman, A. L., Transient Analysis of Electric Power Circuits Handbook. Springer Science and Business Media, 2006.

[20] Das, J. C., Transients in Electrical Systems Analysis, Recognition and Mitigation. McGraw-Hill Professional Publishing, 2010.

[21] ECE 524: Transients in Power Systems, Lecture 27: Development of multiphase line models, University of Idaho, Idaho, USA, 2018.

[22] Goswami, J. C. and Chan, A. K., Fundamentals of Wavelets Theory, Algorithms and Applications, 2nd ed.

[DOR: 20.1001.1.23452951.1400.11.4.6.5]

[DOI: 10.22052.11.4.48]

Vol. 233. John Wiley and Sons, 2011.

[23] IEEE Std C37.114, IEEE Guide for Determining Fault Location on AC Transmission and Distribution Lines, 2014.

[DOR: 20.1001.1.23452951.1400.11.4.6.5]

[DOI: 10.22052.11.4.48]